Chaos Near Structural Phase Transition

H. Beige and M. Diestelhorst

Sektion Physik, Martin-Luther-Universität Halle-Wittenberg, Halle (Saale), German Democratic Republic

R. Forster, J. Albers, and J. Petersson

Fachbereich Physik, Universität des Saarlandes, Saarbrücken, Federal Republic of Germany

Z. Naturforsch. **45a**, 958–964 (1990); received May 30, 1990

An experimental model of a Duffing oscillator is presented. It consists of a linear inductance, a resistance and a ferroelectric nonlinear capacitance. A computer controlled measuring system recorded quantitatively the phase portrait of this series-resonance circuit. The comparison of experimentally observed phase portraits with those calculated by a computer allows to check different assumptions about the nature of the nonlinear properties.

1. Introduction

A widely investigated nonlinear dynamical system is the so called Duffing oscillator (e.g. [1–6]). It offers a great variety of bifurcation cascades. In this paper a Duffing oscillator is represented by a series-resonance circuit, consisting of a linear inductance and a nonlinear capacitance. A ferroelectric triglycine sulfate crystal (TGS) was used as nonlinear capacitance. The structural phase transition in TGS provides the possibility of varying the dielectric properties of the resonator in a large range by merely changing the temperature of the sample.

The aim of the present paper is to show that monitoring the phase portrait of the series-resonance circuit is a useful tool for the study of the nonlinear dielectric properties of TGS above and below the temperature of the phase transition.

A computer controlled measuring system recorded quantitatively the phase portrait of the resonance circuit. Furthermore, different methods were used to determine the dielectric nonlinear coefficient. From a comparison of calculated and observed phase portraits the parameters of the Duffing equation are determined. We discuss the question which information is provided by the phase portrait.

2. The Dielectric Nonlinear Series-Resonance Circuit

Our series-resonance circuit consists of a linear inductance L_0 and the dielectric nonlinear capacitance C_{NL} (see Figure 1). R_s describes the loss of the resonance circuit. The resonance circuit is driven by a sinusoidal voltage $U_0 \cos \omega_e t$. The following differential equation describes the behaviour of the circuit:

$$\ddot{D}_2 + \frac{R_s}{L_0} \dot{D}_2 + \frac{a}{b\,l\,L_0} E_{NL} = \frac{1}{b\,l\,L_0} U_0 \cos \omega_e t\,. \qquad (1)$$

Here D_2 is the dielectric displacement, a the thickness, l the length and b the width of the sample. The electric field strength E_{NL} at the crystal along the ferroelectric axis is a nonlinear function of the dielectric displacement. It may be derived (e.g. [7]) by means of the Landau-theory:

$$E_{NL} = A\,D_2 + B D_2^3 \quad \text{with} \quad A = A_0(\vartheta - \vartheta_0), \quad (2)$$

where A_0 and B are positive constants and ϑ is the temperature. In the case of TGS the value of the Curie-temperature is $\vartheta_c = 49\,^\circ\text{C}$. Inserting (2) into (1)

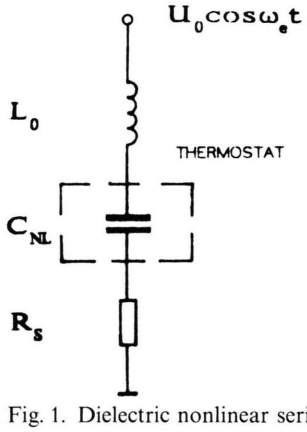

Fig. 1. Dielectric nonlinear series-resonance circuit.

Reprint requests to Prof. Dr. H. Beige, Sektion Physik, Universität Halle-Wittenberg, Halle, Saale, DDR.

0932-0784 / 90 / 0800-0958 $ 01.30/0. – Please order a reprint rather than making your own copy.

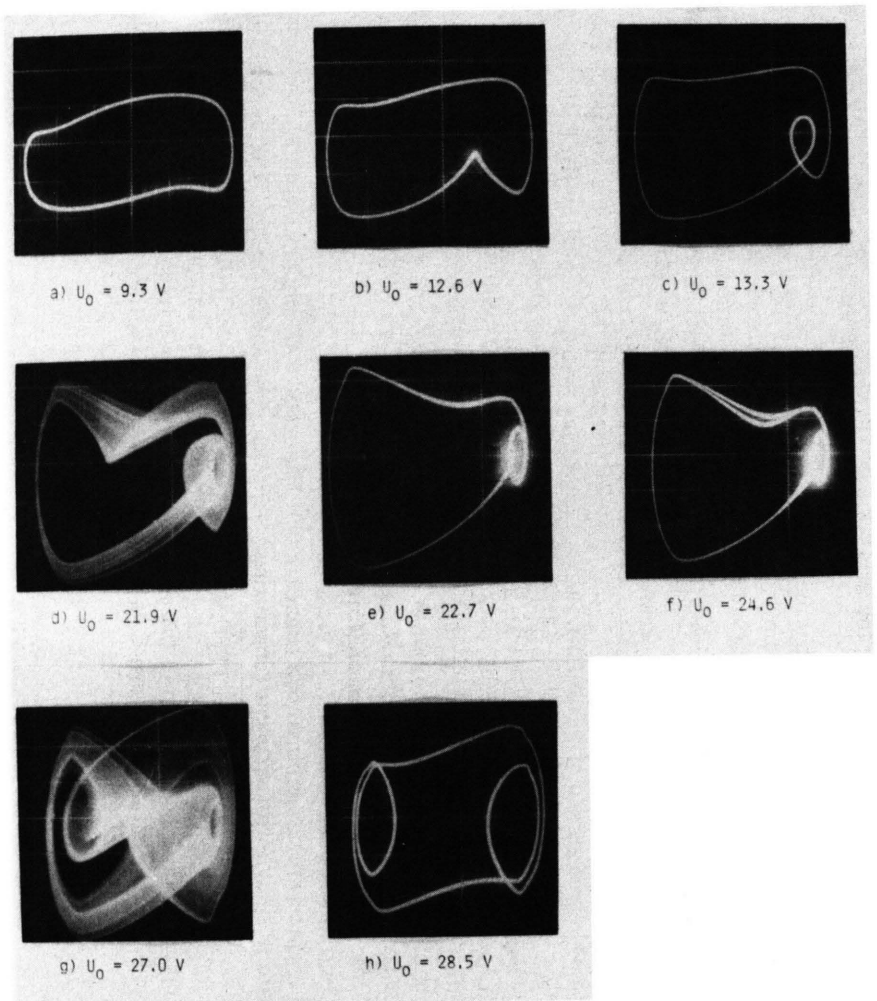

Fig. 2. Phase portrait of the series-resonance circuit at different driving voltages U_0 below the phase transition point.

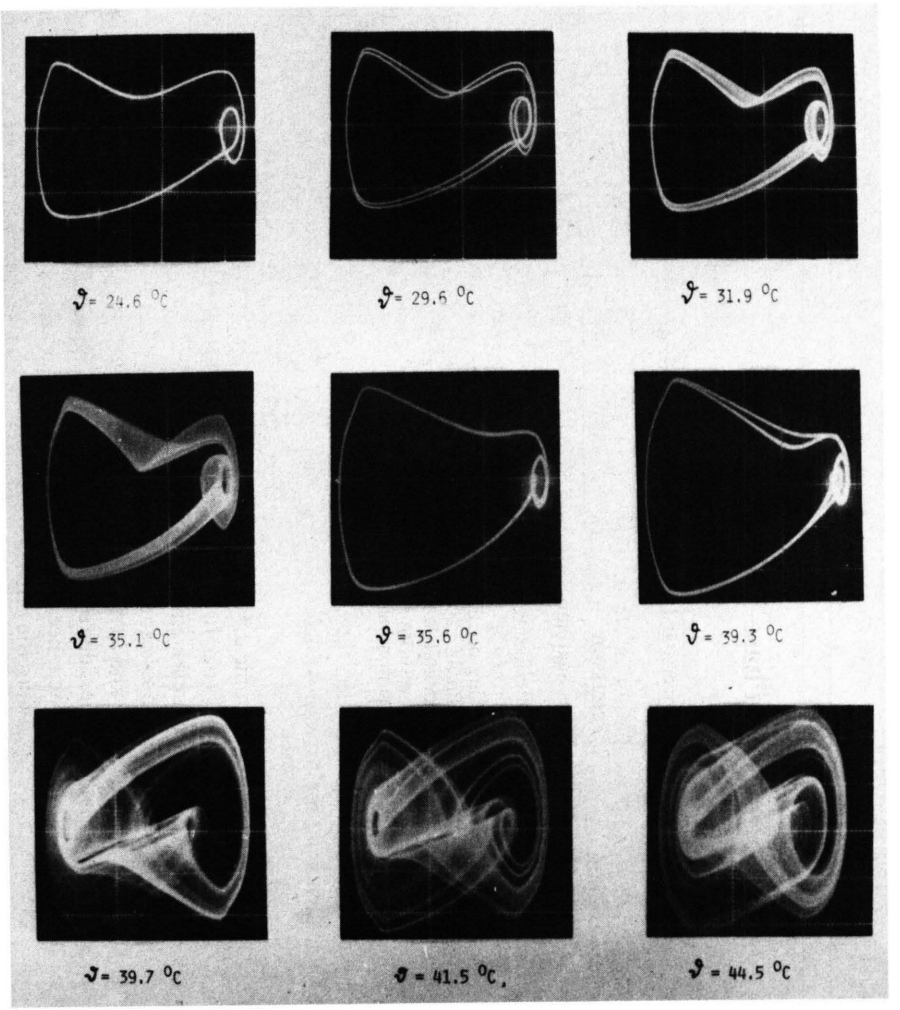

Fig. 3. Phase portraits of the series-resonance circuit at different temperatures.

provides the Duffing-equation

$$\ddot{D}_2 + \frac{R_s}{L_0}\dot{D}_2 + \frac{a\,A}{b\,l\,L_0} D_2 + \frac{a\,B}{b\,l\,L_0} D_2^3 = \frac{U_0}{b\,l\,L_0} \cos \omega_e t. \tag{3}$$

At temperatures above ϑ_c an oscillation of D_2 in a potential with one minimum may be observed. Below ϑ_c the potential becomes a double-well one. In order to compare calculated and observed phase portraits it is necessary to determine all coefficients of (3).

In the case of paraelectric TGS the measurement of the dielectric permittivity and the quality factor of the resonance circuit may be used to determine the coefficients A and R_s/L_0, respectively [8, 11]. The coefficient B was calculated from the shift of the resonance frequency in dependence on the driving voltage U_0:

$$\Delta\omega_e = \frac{3Q^2\,\omega_{0e}\,B}{8a^2\,A^3} U_0^2, \tag{4}$$

where ω_{0e} is the resonance frequency at small voltages U_0 and Q is the quality factor of the circuit. In the case of ferroelectric TGS the coefficients A and B where determined from the relations for the spontaneous polarization

$$D_{2sp} = \pm\sqrt{\frac{A}{B}}. \tag{5}$$

and for the coercive field strength

$$E_{coer} = \pm\frac{2}{3} A \sqrt{\frac{A}{3B}}. \tag{6}$$

These values could be measured from the hysteresis loop of the TGS-crystal.

3. Experimental Representation of Phase Portraits

The first phase portraits were recorded by an analogue measuring system [9–11]. Figure 2 shows phase portraits of the series-resonance circuit at different driving voltages U_0 below the phase transition point. Figure 3 provides the phase portraits of the resonance circuit at different temperatures below the phase transition with constant exciting voltage U_0. In order to reduce heating effects in the sample, a computer controlled measuring system with very short measuring time for a quantitative recording of the phase portrait was developed.

Figure 4 represents the block diagram of the measuring system. Across the linear capacitance C_0 a signal proportional to the dielectric displacement D_2 is recorded. It is possible to vary the temperature of the nonlinear capacitance C_{NL}. A variation of temperature causes mainly a change in the $\frac{B}{A}$ and $\frac{U_0}{A}$ ratios. Further, the amplitude and frequency of the driving voltage can be changed. The measuring system is based on a fully programmable true dual-channel digitizer (Sony/Textronic RTD 710). The digitizer provides 10-bit resolution at a 200 MHz maximum sampling rate (single-channel mode). The data memory is provided by 64 K words (10 bits per word) of a local high-speed RAM. The generator (Philips PM 5192) is fully programmable. With the computer controlled measuring system coupled by IEEE 488 bus the following measuring sequence can be realized:

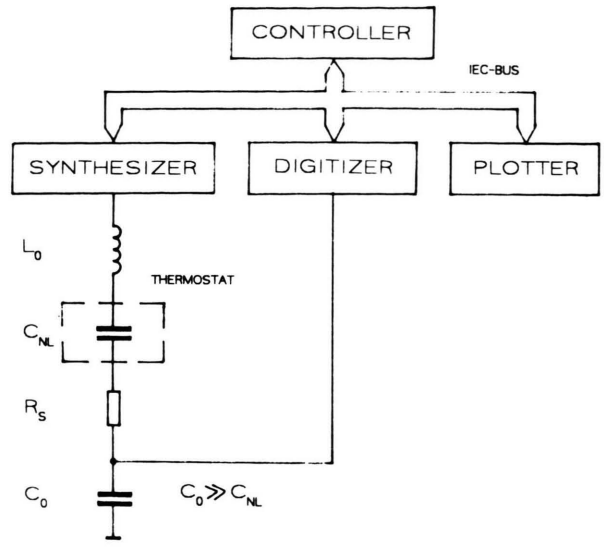

Fig. 4. Block diagram of the measuring system for recording the phase portrait.

- Switch on the exciting voltage
- Record the response of the system (here a delay, in order to obtain the stationary state, or transient oscillations of the series-resonance circuit may be selected
- Switch off the exciting voltage.

Figures 5–7 are obtained with this device. Figure 5 represents the excitation $U(t)$, the response function $D_2(t)$ and the phase portrait $\dot{D}_2 = \dot{D}_2(D_2)$, where $\dot{D}_2$ is calculated by the computer. By removing the inductance L_0 the hysteresis loop may be recorded at the same frequency as the phase portrait. The measuring

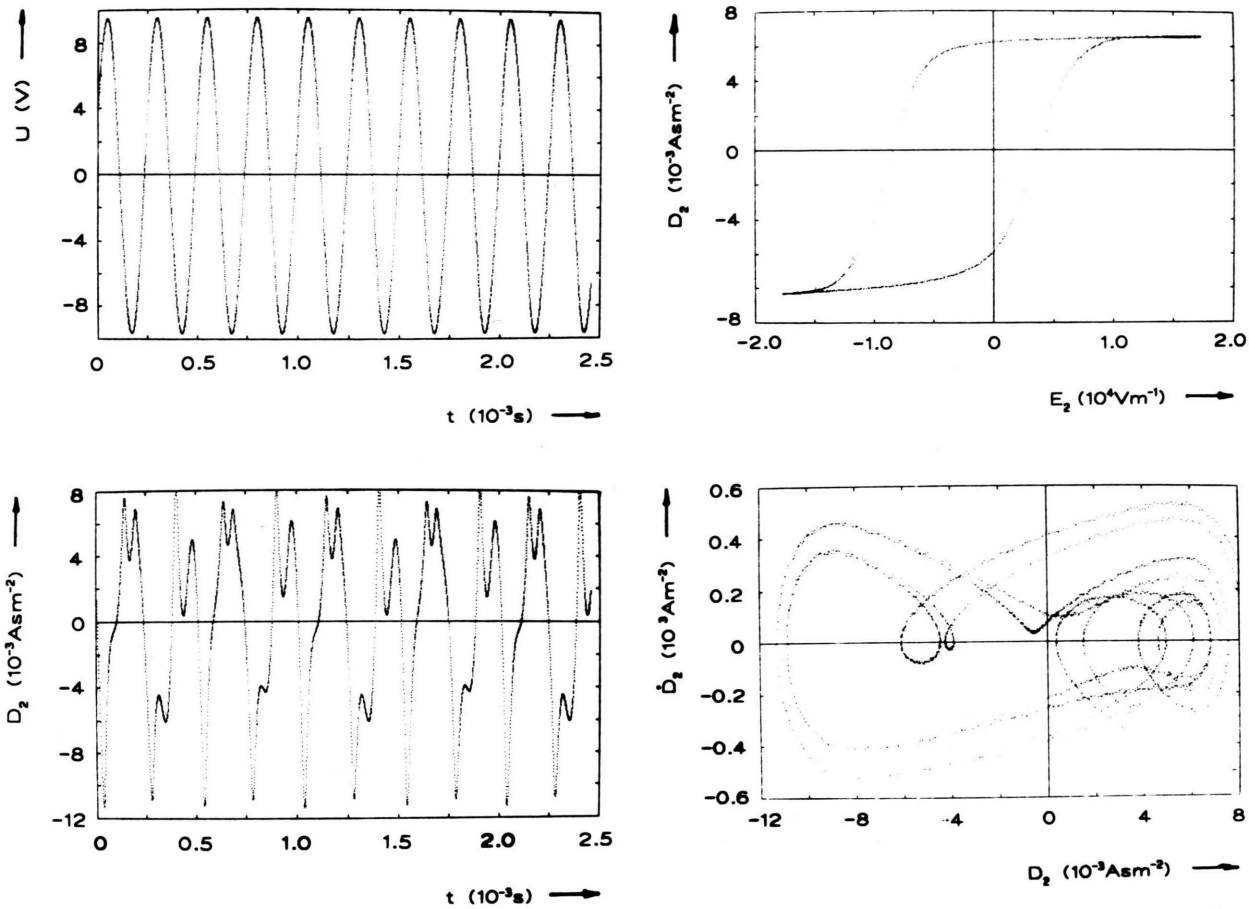

Fig. 5. Experimentally recorded excitation, hysteresis loop, response function and phase portrait below ϑ_c.

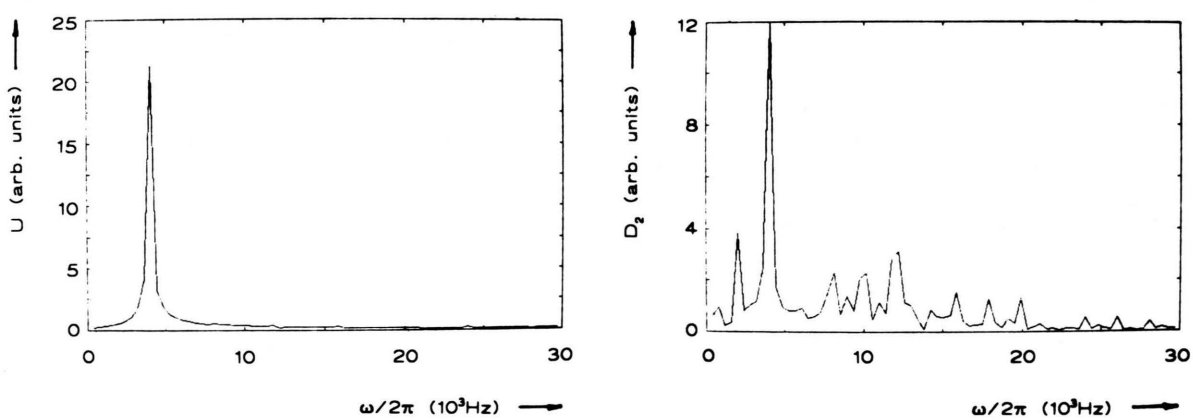

Fig. 6. Fourier spectra of the excitation and of the response function D_2 (amplitude in arbitrary units).

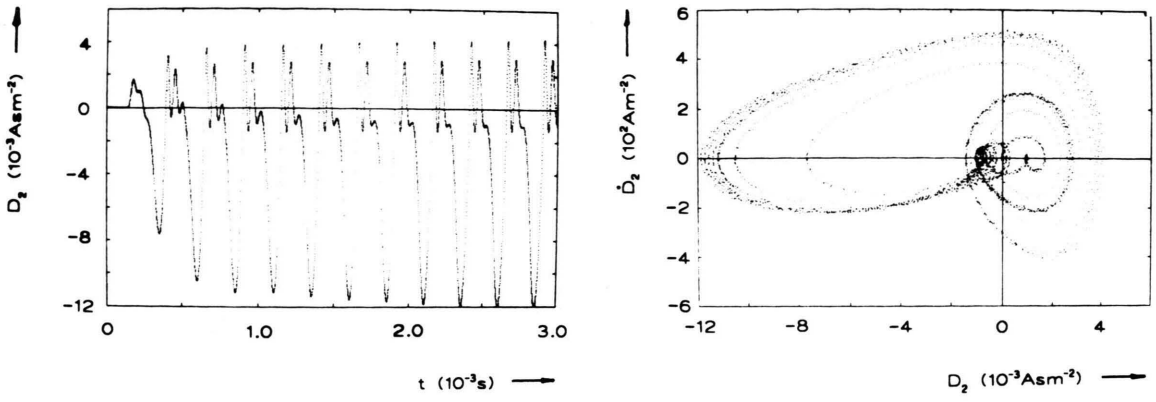

Fig. 7. Experimentally determined response function and phase portrait of transient oscillations.

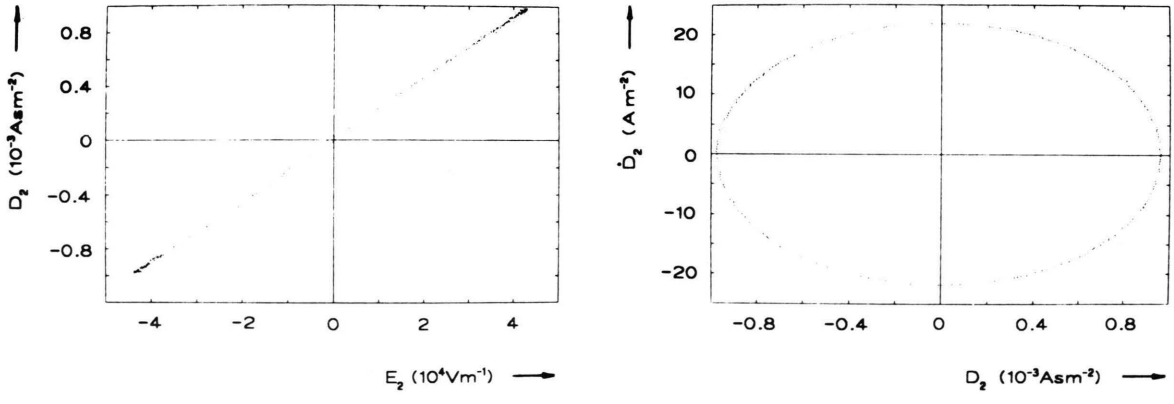

Fig. 8. Experimentally determined relation $D_2 = D_2(E_2)$ and phase portrait above ϑ_c.

time is 2.5 ms. Furthermore, the calculated Fourier spectra of the excitation and of the response function D_2 (see Fig. 6) can be obtained. Figure 7 shows the response function of a transient oscillation.

4. Numerical Calculation of Phase Portraits

In order to calculate the phase portraits above and below the phase transition temperature the nonlinear differential equation is to be solved. In the paraelectric phase we used the value of the nonlinear dielectric coefficient determined by measuring the shift of the resonance frequency in dependence on the amplitude of the excitation. In the ferroelectric phase the computer simulation was carried out with values of the coefficients A and B determined according to (5) and (6). The results of the computer simulation were represented in a form corresponding to the measured records.

5. Comparison of Calculated and Observed Phase Portraits

The phase portraits of the series-resonance circuit were recorded at different temperatures above and below the phase transition.

Figure 8 shows the experimentally determined relation $D_2 = {}_2(E_2)$ and the phase portrait at the temperature $\vartheta = 49.85\,^{\circ}\mathrm{C}$. At the same temperature the following coefficients of the Duffing equation (3) are determined experimentally [12]:

$Q = 44.52$, $U_0 = 23.0\ \mathrm{V}$

$\omega_{0e} = 2\pi \cdot 25\,820\ \mathrm{s}^{-1}$, $a = 0.55 \cdot 10^{-3}\ \mathrm{m}$,

$A = 4.28 \cdot 10^{7}\ \mathrm{VmA}^{-1}\,\mathrm{s}^{-1}$, $\omega_e = 2\pi \cdot 4000\ \mathrm{s}^{-1}$.

$B = 3.44 \cdot 10^{11}\ \mathrm{Vm}^{5}\,\mathrm{A}^{-3}\,\mathrm{s}^{-3}$,

The results of the computer simulation with these coefficients and the experimentally observed phase portraits are quantitatively in good agreement.

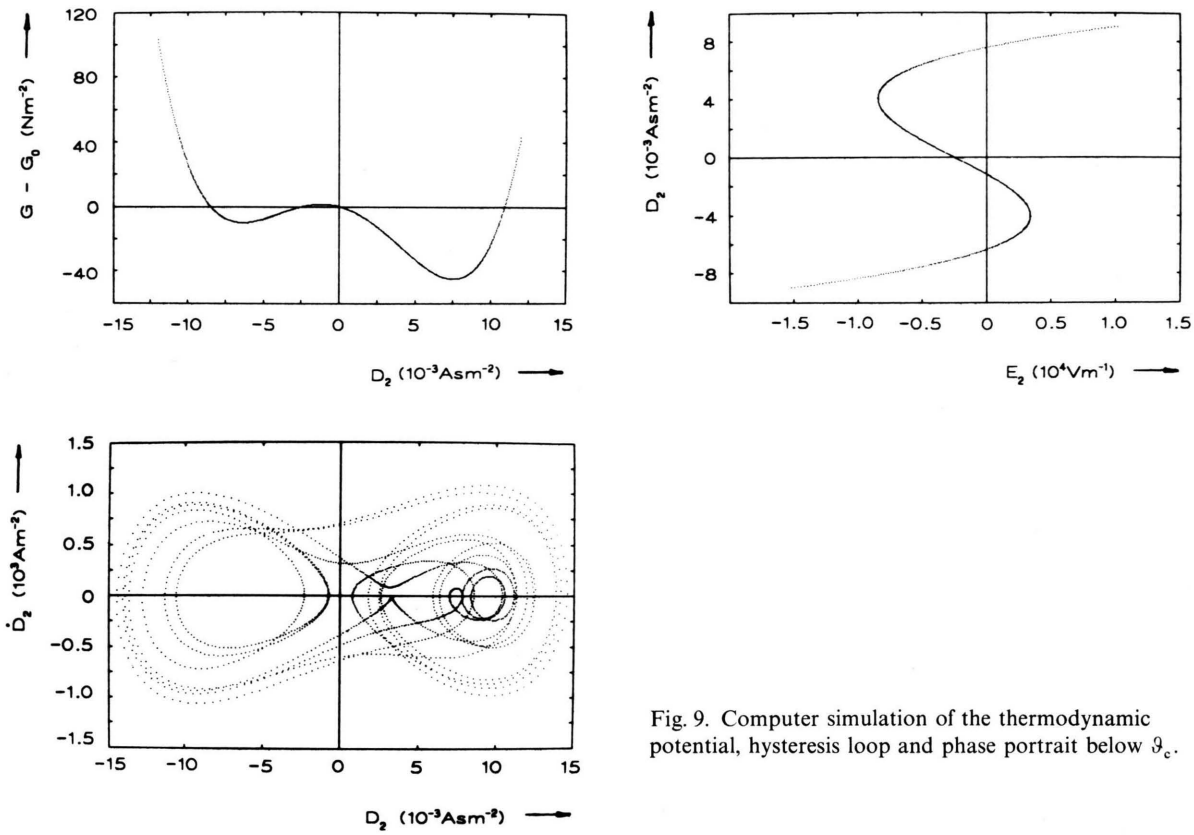

Fig. 9. Computer simulation of the thermodynamic potential, hysteresis loop and phase portrait below ϑ_c.

Figures 5–7 show the experimental results below the phase transition at the temperature $\vartheta = 45.26\,^{\circ}\mathrm{C}$. At the same temperature the coefficients of the Duffing equation (3) are determined experimentally and the corresponding simulation is carried out.

The hysteresis loop (see Fig. 5) was recorded and the coefficients A and B were determined by the values of the spontaneous polarization (5) and of the coercive field strength (6). The coefficients A and B derived from the hysteresis loop become

$$A = -2.18 \cdot 10^{6}\ \mathrm{VmA^{-1}\,s^{-1}},$$

$$B = \ \ 4.44 \cdot 10^{10}\ \mathrm{VmA^{-3}\,s^{-3}}.$$

Figure 9 shows the result of the computer simulation with these coefficients. The influence of an internal bias field ($E_{=} = 2500$ V/m) is added. In this case the thermodynamic potential

$$G = G_0 + \frac{A}{2} D_2^2 + \frac{B}{4} D_2^4 - E_{=} D_2$$

is used. The calculated and observed phase portraits agree well with the computer simulation derived from the hysteresis loop. By measuring the hysteresis loop and the phase portrait the influence of the domain reorientation on the nonlinear dielectric properties is observed.

The conclusion that phase portraits provide information about the "effective thermodynamic potential" is supported by the high sensitivity of the phase portraits against a bias field at the sample. Figure 10 represents the influence of a very small bias field $E_{=} = \pm 2720$ V/m on the phase portrait in the ferroelectric phase.

8. Summary

The experimentally obtained phase portrait provides additional information about the nonlinear dynamical behaviour near the structural phase transition. With knowledge of the linear and nonlinear

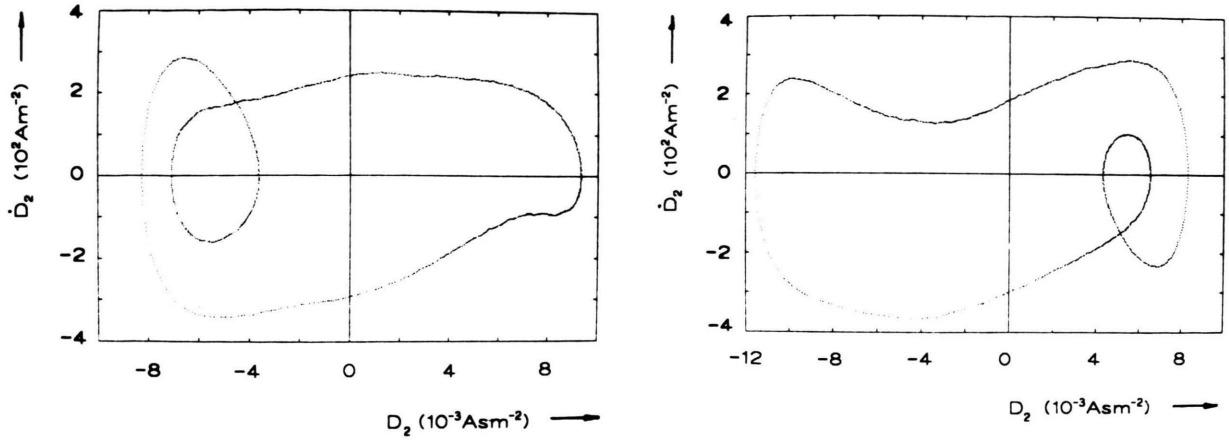

Fig. 10. Influence of a bias field on the phase portrait in the ferroelectric phase.

properties of the system it is possible to obtain the phase portrait with a computer. Particularly the comparison of calculated and experimental phase portraits yields hints about the nature of the nonlinear properties and underlying physical mechanisms. The record of the phase portrait provides the opportunity to investigate the nonlinear dynamics in dependence on the frequency in order to study for example switching processes in ferroelectric and ferroelastic materials.

An advantage of measurements compared to numerical simulations is the possibility to ascribe the nonlinear phenomena to particular physical effects, that means in our case to dielectric nonlinearities in a ferroelectric crystal near the phase transition.

[1] A. H. Nayfeh and D. T. Mook, Nonlinear Oscillations, New York 1979.
[2] Y. Ueda, J. Stat. Phys. **20,** 181 (1979).
[3] R. Seydel, Physica **17** D, 308 (1985).
[4] S. Martin, H. Leber, and W. Martienssen, Phys. Rev. Lett **53,** 303 (1984).
[5] U. Parlitz and W. Lauterborn, Phys. Lett. **107** A, 351 (1985).
[6] U. Parlitz and W. Lauterborn, Z. Naturforsch. **41 A,** 605 (1986).
[7] M. E. Lines and A. M. Glass, Principles and Applications of Ferroelectrics and Related Materials, Oxford 1979.
[8] H. Beige and G. Schmidt, Ferroelectrics **41,** 173 (1982).
[9] H. Beige, J. Albers, and J. Petersson, Japan J. Appl. Phys. **24,** Suppl. 24-2, 715 (1985).
[10] M. Diestelhorst and H. Beige, Ferroelectrics **81,** 979 (1988).
[11] M. Diestelhorst, Ferroelektrizität '87, WB MLU 67 (024) (1987), p. 68.
[12] M. Diestelhorst, R. Hofmann, and H. Beige, Japan J. Appl. Phys. **24,** (Suppl. 24-2) 1019 (1985).